Disinhibitory and neuromodulatory regulation of hippocampal synaptic plasticity

Inês Guerreiro[1], Zhenglin Gu[2], Jerrel L. Yakel[2], Boris S. Gutkin[1,3]

[1] Group for Neural Theory, LNC2 INSERM U960, DEC Ecole Normale Superieure PSL University, Paris 75005, France

[2] Neurobiology Laboratory, National Institute of Environmental Health Sciences, National Institutes of Health, Department of Health and Human Services, Research Triangle Park, NC 27709, USA

[3] Center for Cognition and Decision Making, Institute for Cognitive Neuroscience, NRU Higher School of Economics, Moscow 101000, Russia

Abstract

Hippocampal synaptic plasticity, particularly in the Schaffer collateral (SC) to CA1 pyramidal excitatory transmission, is considered as the cellular mechanism underlying learning. The CA1 pyramidal neurons are embedded in an intricate local circuitry that contains a variety of interneurons. The roles these interneurons play in the regulation of the excitatory synaptic plasticity remains largely understudied. Our recent experiments showed that repeated cholinergic activation of α7 nACh receptors expressed in oriens-lacunosum-moleculare (OLMα2) interneurons could induce LTP in SC-CA1 synapses, likely through disinhibition by inhibiting stratum radiatum (s.r.) interneurons that provide feedforward inhibition onto CA1 pyramidal neurons, revealing a potential mechanism for local interneurons to regulate SC-CA1 synaptic plasticity. Here, we pair *in vitro* studies with biophysically-based modeling to uncover the mechanisms through which cholinergic-activated GABAergic interneurons can disinhibit CA1 pyramidal cells, and how repeated disinhibition modulates hippocampal plasticity at the excitatory synapses. We found that α7 nAChR activation increases OLM activity. OLM neurons, in turn inhibit the fast-spiking interneurons that provide feedforward inhibition onto CA1 pyramidal neurons. This disinhibition, paired with tightly timed SC stimulation, can induce potentiation at the excitatory synapses of CA1 pyramidal neurons. Our work further describes the pairing of disinhibition with SC stimulation as a general mechanism for the induction of hippocampal synaptic plasticity.

Disinhibition of the excitatory synapses, paired with SC stimulation, leads to increased NMDAR activation and intracellular calcium concentration sufficient to upregulate AMPAR permeability and potentiate the synapse. Repeated paired disinhibition of the excitatory synapse leads to larger and longer lasting increases of the AMPAR permeability. Our study thus provides a novel mechanism for inhibitory interneurons to directly modify glutamatergic synaptic plasticity. In particular, we show how cholinergic action on OLM interneurons can down-regulate the GABAergic signaling onto CA1 pyramidal cells, and how this shapes local plasticity rules. We identify paired disinhibition with SC stimulation as a general mechanism for the induction of hippocampal synaptic plasticity.

Introduction

Since the discovery of long-term potentiation (LTP) in the hippocampus in 1973, this structure has been used as a model to study the mechanisms of synaptic plasticity induction (Bliss, 1973). The hippocampal SC to CA1 synapses are among the most studied for synaptic plasticity. The majority of the work has focused on excitatory glutamatergic transmission. However, recent work has shown the importance of inhibitory inputs in the modulation of local hippocampal synaptic plasticity (Saudargiene & Graham, 2015; Chevaleyre & Piskorowski, 2014; Wigstrom & Gustafsson, 1985).

The hippocampal network comprises a large variety of locally connected GABAergic interneurons exerting powerful control on network excitability. GABAergic interneurons receive important cholinergic innervation from the medial septum and are endowed with a variety of different subtypes of nicotinic acetylcholine receptors (nAChRs) that are thought to be involved in regulating excitability, plasticity, and cognitive functions (Griguoli & Cherubini, 2012; Levin, 2002; Yakel, 2012). However, the mechanisms through which cholinergic-activated GABAergic interneurons modulate excitatory transmission and induction of hippocampal plasticity at excitatory synapses remain largely unclear.

Alterations of cholinergic action on hippocampal GABAergic interneurons have been implicated in cognitive dysfunction in Alzheimer's disease (AD) (Schmid, et al., 2016). Understanding how cholinergic activation of GABAergic interneurons regulates hippocampal excitability and induces synaptic plasticity will provide insight for understanding higher brain functions, namely memory impairment, with potential relevance for AD treatments.

Previous studies showed that activation of OLMα2 interneurons increases SC to CA1 transmission, likely through disinhibition by reducing the activity of stratum radiatum (s.r.) interneurons that in turn provide feed-forward inhibition onto pyramidal neurons (Leão, et al., 2012). Consistent with these studies, Gu et al. found that activation of OLMα2 interneurons increased SC to CA1 EPSCs and reduced IPSCs (Gu, et al., 2020). However, the mechanisms through which the activation of the inhibitory interneurons OLMα2 is regulating the activity of inhibitory interneurons targeting the CA1 pyramidal cell, and how this facilitates the potentiation of SC-evoked EPSPs of the CA1 pyramidal cells, remain elusive.

In this work, we use a minimal biophysical circuit model, driven quantitatively by in vitro data, to examine how activation of OLM cells modulates the activity of fast-spiking interneurons whose GABAergic inputs are co-localized with the SC glutamatergic synapses onto a CA1 pyramidal cell dendrite , and how this promotes the induction of plasticity at the SC-CA1 synapse. More specifically, we seek to determine how cholinergic activation of the OLM cells through the post-synaptic α7 nAChRs can down-regulate the GABAergic signaling onto the pyramidal cells, and how a decrease in inhibitory inputs to the pyramidal cells can modulate the plasticity of the excitatory SC-CA1 synapse. We thus constructed a minimal circuit consisting of a single compartment spiking model of an OLM interneuron with postsynaptic α7 nAChRs, a fast-spiking interneuron with postsynaptic AMPA and $GABA_A$ receptors, and a pyramidal cell dendritic compartment with postsynaptic AMPA, NMDA and $GABA_A$ receptors, connected as schematically shown in Figure 1.

It is currently well accepted that LTP triggering processes require calcium influx through NMDARs. At the same time, LTP has been associated with changes in the properties of postsynaptic AMPARs; namely changes in their number and phosphorylation state (Barria, Muller, Derkach, Griffith, & Soderling, 1997; Collingridge, Kehl, & McLennan, 1983; Lüscher & Malenka, 1994) . To reflect these mechanisms, we employ the calcium-based synaptic plasticity model (proposed by Shouval et al. (Shouval, Bear, & Cooper, 2002)) to model synaptic plasticity of the SC-CA1 excitatory synapse. We describe how a decreased release of the inhibitory neurotransmitter GABA could lead to increased NMDAR activation and intracellular calcium concentration, leading to changes in the CA1 pyramidal cell postsynaptic AMPA-mediated conductance. Our work also shows how nicotinic cholinergic action on OLM interneurons can downregulate the GABAergic signaling onto CA1 pyramidal cells and facilitate potentiation of the SC-CA1 synapse.

79 [Figure 1]

80

81

82 ## Methods

83 ### Animals and materials

84 All procedures related to the use of mice followed protocols approved by the Institutional Animal Care and Use
85 Committees of the NIEHS. ChAT-cre mice (B6;129S6-Chattm2(cre)Lowl/J), Sst-cre mice (Ssttm2.1(cre)Zjh), and floxed
86 α7 nAChR knockout mice (B6(Cg)-Chrna7tm1.1Ehs/YakelJ) were originally purchased from Jackson Laboratory and
87 then bred at NIEHS. OLMα2-cre mice (Tg(Chrna2cre)OE29Gsat/Mmucd) were originally obtained from Mutant Mouse
88 Resource and Research Centers (MMRRC) and then bred at NIEHS. Mice (of either sex) were used for slice culture
89 from day 6 to 8.
90 Culture media were from Sigma and Invitrogen. AAV serotype 9 helper plasmid was obtained from James Wilson at
91 the University of Pennsylvania. The AAV vector containing floxed ChR2 (Addgene #20297) and floxed eNpHR
92 (Addgene #26966) were obtained from Karl Deisseroth (Witten et al., 2010; Gradinaru et al., 2010). AAV viruses were
93 packaged with serotype 9 helper at the Viral Vector Core facility at NIEHS.

94

95 ### Brain slice culture and AAV virus infection

96 To study the effects of cholinergic coactivation on the plasticity of SC to CA1 synapses in Figure 2, coronal septal slices
97 (350 μm) from ChAT-cre mice and horizontal hippocampal slices from floxed α7 nAChR mice or OLMα2-cre/floxed α7
98 nAChR mice (350 μm) were cut with Leica VT1000S vibratome. Medial septal tissue containing cholinergic neurons
99 was then dissected out and placed next to the hippocampus on a 6-well polyester Transwell insert (Corning) and
100 cultured there for about 2 weeks before being used for experiments, similar as previously described (Gu and Yakel,
101 2017). AAV viruses containing double floxed ChR2 construct (5 nl) were microinjected to the septal tissue with a
102 micro injector (Drummond Scientific) on the second day of culturing. To study the effects of disinhibition on the
103 plasticity of SC to CA1 synapses in Figure 4, horizontal hippocampal slices from Sst-cre mice were cultured and AAV

104 viruses containing double floxed eNpHR construct were microinjected to the hippocampus the next day.

105

106 **Whole-cell patch clamp recordings**

107 SC to CA1 excitatory post-synaptic currents (EPSCs) were recorded from hippocampal CA1pyramidal neurons under
108 whole-cell patch clamp, similar as described before (Gu and Yakel, 2011, 2017). Briefly, 2-3 weeks after culturing, the
109 slices were removed from transwell inserts and put into a submerged chamber, continuously perfused with
110 95%O_2/5%CO_2 balanced ACSF (in mM, 122 NaCl, 2.5 KCl, 2 $MgCl_2$, 2 $CaCl_2$, 1.2 NaH_2PO_4, 25 $NaHCO_3$, 25 glucose) at
111 room temperature. EPSCs were recorded at -60 mV under voltage clamp through a glass pipette filled with internal
112 solution (in mM, 130 potassium gluconate, 2 $MgCl_2$, 3 MgATP, 0.3 Na_2GTP, 10 KCl, 10 HEPES, and 1 EGTA, with pH
113 ~7.2-7.3 and osmolarity ~280-290 mOsm). Whole-cell patch clamp recordings were performed with Multiclamp 700B
114 amplifier (Axon Instruments). Data were digitized with Digidata 1550, collected with Clampex. The amplitudes of
115 EPSCs were analyzed with Clampfit and graphs were drawn with Excel. The amplitudes were normalized to the mean
116 of the 10-min baseline recording before cholinergic pairing or disinhibition pairing. Values were presented as mean
117 ± SEM.

118 EPSCs were evoked every 60 seconds by stimulating the SC pathway with an electrode placed in the stratum radiatum
119 through a stimulator (Grass S88X). The stimulation intensity was 1-10 µA for 0.1 ms. To study the effects of cholinergic
120 coactivation on SC to CA1 synaptic plasticity in Figure 2, cholinergic terminals in the hippocampus were
121 optogenetically activated (10 pulses at 10 Hz, 1 sec before SC stimulation) through ChR2 that was selectively
122 expressed in ChAT-cre positive (cholinergic) neurons. ChR2 was activated with 488-nm laser light (20 ms) through a
123 40× objective with an Andor spinning disk confocal microscope (Andor technology). To study the effects of
124 disinhibition on SC to CA1 synaptic plasticity in Figure 4, Sst positive neurons were inhibited optogenetically through
125 eNpHR which was activated with 530-nm laser light for 1 sec over SC stimulation.

126

127 **Model**

128 The minimal network used in this study consists of an OLM cell (O), a fast-spiking interneuron (I), and a pyramidal
129 cell. All the cells in the network are modeled as point neurons. Since we are interested in studying local changes at

the SC-CA1 synapse, the pyramidal cell is represented by a dendritic compartment (E_D).

Neuron dynamics models

The O and I cells are modeled using the standard Hodgkin-Huxley currents (Hodgkin & Huxley, 1952) (transient I_{Na}, delayed rectifier potassium I_K, and leak I_{leak}), with synaptic currents I_{syn}. Its membrane potential V_m is described as follows:

$$C_m \frac{dV_m}{dt} = -I_{leak} - I_K - I_{Na} - I_{syn} \tag{1}$$

where C_m is the membrane capacitance. The I_{leak}, I_K and I_{Na} currents are given by:

$$I_{leak} = g_{leak}(V_m - E_{leak}) \tag{2}$$

$$I_K = \bar{g}_K n^4 (V_m - E_K) \tag{3}$$

$$I_{Na} = \bar{g}_{Na} m^3 h \tag{4}$$

here $\bar{g}_i$ and E_i are, respectively, the maximal conductance and reversal potential of channel i (i=leak, K, Na), and m, h and n are gating variables that obey the following differential equation:

$$\frac{dx}{dt} = \alpha_x (1 - x) - \beta_x \tag{5}$$

where α_x and β_x are voltage-dependent rate constants.

In addition, the O-cells have an applied current $I_{app} = -2.6\ \mu A/cm^2$, a persistent Na-current I_p, and a hyperpolarization-activated inward current I_h (with a slow and fast component), as described in (Rotstein, et al., 2005):

$$I_p = \bar{g}_p p\ (V_m - E_{Na}) \tag{6}$$

$$I_h = \bar{g}_h (0.65 h^f + 0.35 h^s)(V_m - E_h) \tag{7}$$

While the gate variable p obeys equation (5), h^f and h^s are described by the following equation:

$$\frac{dx}{dt} = \frac{x_\infty(V_m) - x}{\tau_x(V_m)} \tag{8}$$

where x_∞ is the voltage dependent steady state and τ_x the time constant. Definitions for the α_x, β_x, x_∞ and τ_x for each of the dynamic variables are as follows.

For the O-cells:

$$\alpha_n = \frac{-0.01(V_m + 27)}{exp\big(-0.1(V_m + 27)\big) - 1}$$

$$\beta_n = 0.125\, exp\left(-\frac{V_m + 37}{80}\right)$$

$$\alpha_m = \frac{-0.1(V_m + 23)}{exp\big(-0.1(V_m + 23)\big) - 1}$$

$$\beta_m = 4exp\,(-\frac{V_m + 48}{18})$$

$$\alpha_h = 0.07exp\,(-\frac{V_m + 37}{20})$$

$$\beta_h = \frac{1}{exp\,(-0.1(V_m + 7) + 1)}$$

$$\alpha_p = \frac{1}{0.15(1 + exp\,(-\frac{V_m + 38}{6.5}))}$$

$$\beta_p = \frac{exp\left(-\frac{V_m + 38}{6.5}\right)}{0.15(1 + exp\,(-\frac{V_m + 38}{6.5}))}$$

$$h_\infty^f = \frac{1}{1 + exp\left(\frac{V_m + 79.2}{9.78}\right)}$$

$$\tau_h^f = \frac{0.51}{exp\left(\frac{V_m - 1.7}{10}\right) + exp\,(-\frac{V_m + 340}{52})} + 1$$

$$h_{\infty}^{s} = \frac{1}{\left[1 + exp\left(\frac{V_m + 2.83}{15.9}\right)\right]^{58}}$$

$$\tau_h^s = \frac{5.6}{exp\left(\frac{V_m - 1.7}{14}\right) + exp\,(-\frac{V_m + 260}{43})} + 1$$

For the I-cells:

$$\alpha_n = \frac{0.032(V_m + 52)}{1 - \ exp\left(-\frac{V_m + 52}{5}\right)}$$

$$\beta_n = 0.5\,exp\left(-\frac{V_m + 57}{40}\right)$$

$$\alpha_m = \frac{0.32(V_m + 54)}{1 - \ exp\left(-\frac{V_m + 54}{4}\right)}$$

$$\beta_m = \frac{0.28(V_m + 27)}{exp\left(\frac{V_m + 27}{5}\right) - 1}$$

$$\alpha_h = 0.128exp\,(-\frac{V_m + 50}{18})$$

$$\beta_h = \frac{4}{1 + exp\,(-\frac{V_m + 27}{5})}$$

The parameter values used in the simulations are the ones presented in Table 1.

Since we are interested in studying local synaptic changes of the SC-CA1 synapse, we use the following equation to describe the activity of the pyramidal cell dendritic compartment:

(9)

$$C\frac{dV_{E_D}}{dt} = -I_{leak} - I_{syn}$$

The parameters C, g_{leak} and E_{leak} are the same as for the I-cells.

Synaptic models

The O-cells have a synaptic current mediated by pre-synaptic α7 nAChR channels. The description of the current here used is an adaptation of the model proposed in (Graupner & Gutkin, 2013), and it is given by

$$I_{\alpha 7} = \bar{g}_{\alpha 7} r_{\alpha 7}(V_m - E_{\alpha 7}) \tag{10}$$

where $\bar{g}_{\alpha 7}$ is the maximal conductance of the α7 nAChR channel, and $E_{\alpha 7}$ the reversal potential. The opening gate variable $r_{\alpha 7}$ is described by equation (8), with $\tau_{r\alpha 7}$ constant and $r_{(\alpha_7)\infty}$ given by

$$r_{(\alpha_7)\infty} = \frac{[ACh]^n}{EC_{50}^n + [ACh]^n} \tag{11}$$

where EC_{50} is the half-maximum concentration, and *n* the Hill's coefficient of activation.

The I-cell has an excitatory AMPA and inhibitory $GABA_A$ synaptic currents, described by the following set of equations:

$$I_{GABA_A} = \bar{g}_G r_G(V_m - E_G) \tag{12}$$

$$I_{AMPA} = \bar{g}_A r_A(V_m - E_A) \tag{13}$$

The gating variables r_x is, as described in (Destexhe, Mainen, & Sejnowski, 1998), given by

$$\frac{dr_x}{dt} = \alpha_x[T](1 - r_x) - \beta_x r_x \tag{14}$$

where α_x and β_x are the opening and closing rate of the receptor channel, and [T] the neurotransmitter's concentration available for binding.

The GABA release resultant from the respective activation of the O and I-cells depends on its membrane potential

173 V_m according to the following equation:

$$[GABA] = \frac{T_{max}}{1 + \exp\left(-\frac{V_m - V_p}{K_p}\right)} \tag{15}$$

174 where T_{max} is the maximal neurotransmitter concentration, K_p gives the steepness of the function, and V_p sets the

175 value at which the function is half-activated.

176 The dendritic compartment E_D is modeled using synaptic $GABA_A$, AMPA and NMDA currents. The $GABA_A$ and AMPA

177 currents are given by equations (12) and (13), respectively. The NMDA current is described by the following equation:

$$I_{NMDA} = \bar{g}_N r_N B(V_m)(V_m - E_N) \tag{16}$$

178

179 where r_N is the gating variable described by equation (14). Due to the presence of a Mg^{2+} block, the NMDA channels

180 have an extra voltage-dependent term, $B(V_m)$, defined as:

$$B(V_m) = \frac{1}{1 + \exp(-0.062V_m)\frac{[Mg^{2+}]}{3.57}} \tag{17}$$

181 The reversal potentials of the excitatory receptors E_A and E_N are 0 mV, while one of the inhibitory $GABA_A$ receptor is

182 E_G = −80 mV. Postsynaptic AMPA and $GABA_A$ receptors at the I-cell have maximal conductance $\bar{g}_{AMPA} = 0.1\ mS/cm^2$

183 and $\bar{g}_G = 0.6\ mS/cm^2$. at E_D have a maximal conductance of $\bar{g}_{AMPA} = 0.3\ mS/cm^2$. Postsynaptic AMPA, $GABA_A$ and

184 NMDA receptors at E_D have maximal conductances of $\bar{g}_{AMPA} = 0.3\ mS/cm^2$, $\bar{g}_G = 0.42\ mS/cm^2$ and $\bar{g}_N =$

185 $0.4\ mS/cm^2$, except for Figures 2 and 3 where we use $\bar{g}_N = 0.2\ mS/cm^2$ and $\bar{g}_G = 0.7\ mS/cm^2$. The remaining

186 parameters are defined in Table 2.

187

188 **Model of synaptic plasticity**

189 We use a calcium-based synaptic plasticity model based on (Shouval, Bear, & Cooper, 2002). We assume that

190 changes in the AMPA receptor conductance reflect changes in the strength of the excitatory SC-CA1 synapse. Our

synaptic plasticity model is formulated as follows:

$$\frac{d\bar{g}_{AMPA}}{dt} = \eta(Ca)\big(\Omega(Ca) - \sigma(\bar{g}_{AMPA} - 0.3)\big) \tag{18}$$

where σ is a decay constant. The variable η is a calcium-dependent learning rate described by equation (19), and Ω determines the sign magnitude of synaptic plasticity as a function of the intracellular Ca levels (equation (20)).

$$\eta(Ca) = \left(\frac{P_1}{P_2 + Ca^{P_3}} + P_4\right)^{-1} \tag{19}$$

$$\Omega(Ca) = \gamma_p \frac{\exp\left(40\big(Ca - \theta_p\big)\right)}{1 + \exp\left(40\big(Ca - \theta_p\big)\right)} - \gamma_d \frac{\exp\big(40(Ca - \theta_d)\big)}{1 + \exp\big(40(Ca - \theta_d)\big)} \tag{20}$$

The parameters Θ_p and Θ_d define the depression and potentiation threshold, with $\Theta_p > \Theta_d$, and γ_p and γ_d define the potentiation and depression amplitude, with $\gamma_p > \gamma_d$.

We assume that the main source of Ca^{2+} is the calcium flux entering the cell through the NMDA receptor channels. The intracellular Ca^{2+} concentration evolves according to the following equation

$$\frac{dCa}{dt} = -\alpha I_{NMDA} - \frac{Ca}{\tau_{Ca}} \tag{21}$$

where α is the NMDARs permeability to calcium, and τ_{Ca} the calcium decay constant.

The parameter values used in the simulations are the ones presented in Table 3, except for Figure 2 and Figure 3 where $\gamma_p = 0.165$ and $\gamma_d = 0.100$.

207 **Results**

208 **Co-activation of cholinergic and glutamatergic inputs modifies the SC-CA1 synaptic transmission**

209 Previously, it has been observed that coactivation of hippocampal cholinergic inputs and local SC pathway increases
210 the amplitude of SC to CA1 pyramidal EPSCs. Moreover, repeated pairing of cholinergic and hippocampal inputs (8
211 times) induced the enhancement of EPSCs from pyramidal neurons not only during the pairing, but also long after,
212 indicating the induction of long-term synaptic plasticity at SC to CA1 excitatory synapses. The induction of
213 potentiation was abolished by a knock-out of OLMα2 interneuronal α7 nAChRs (Figures 2A and 2C).

214 SC stimulation elicits EPSCs in s.r. interneurons and in the CA1 pyramidal cell dendrites (Leão, et al., 2012). On the
215 other hand, despite the fact that α7 nAChR-mediated currents have been observed in both hippocampal pyramidal
216 neurons and interneurons, only the knockout of α7 nAChRs in OLMα2 interneurons blocked the potentiation of
217 cholinergic-pairing-induced SC-evoked pyramidal cell EPSPs (Gu, et al., 2020). We thus modeled α7 nAChR-mediated
218 modulation of OLM neurons only. We constructed a minimal feed-forward circuit with an OLM cell (O), a fast-spiking
219 interneuron (I), and the pyramidal cell s.r. dendritic compartment (E_D) connected as schematically shown in Figure
220 1B to examine mechanistically how pairing cholinergic activation of the O-cell with glutamatergic activation of the I-
221 cell and E_D can potentiate the EPSCs of E_D. Both the OLM cell and the FS neuron are modelled following a conductance-
222 based Hodgkin-Huxley formalism (see methods). We study how the EPSC of E_D, modelled as the sum of the
223 postsynaptic AMPA and NMDA currents (I_{AMPA} and I_{NMDA}), change when the glutamatergic inputs acting on the I-cell
224 and E_D are paired with the cholinergic inputs that act on the post-synaptic α7 nAChR of to the O-cell during a co-
225 pairing period of 8 minutes, identical to the experimental protocol. Both before, during and after the co-pairing
226 period, the I-cell and E_D receive one pulse of glutamate per minute. During the co-pairing period the O-cell receives
227 a pulse of ACh per minute, 1 msec prior to each glutamate pulse. Not much is known about the concentration profile
228 of ACh in vivo, but it is believed that it can be cleared from the synaptic cleft within milliseconds**.** Therefore, both
229 ACh and glutamate are modeled as square pulses with a duration of 3 msec and 1 mM of amplitude. ACh then acts to
230 activate the α7 nAChRs, producing a depolarising current in the target neuron in our model.

231 From Figure 2D, we see that during the co-pairing period (from t=10 min to t=18 min), the EPSC is increased. This
232 increase in our model is maintained for an extended period of time after the co-pairing period is over (black line),

233 matching the experimental results. We also see that during the co-pairing period, GABA release from the I-cells,
234 $GABA_I$, decreases significantly (see Figure 2D inset). If we decrease the maximal conductance of the α7 nAChR, $g_{\alpha 7}$,
235 from 4 mS/cm^2 to 1 mS/cm^2 (or lower), co-pairing no longer potentiates the EPSC of E_D (orange line). This is in
236 accordance with experimental results that showed that this form of EPSC boost was abolished by knockout of the α7
237 nAChR in OLMα2 interneurons (Figure 2C).
238
239 [Figure 2]
240
241 We then examined how the key parameters of the co-paring protocol influence the plasticity of the SC-CA1 EPSCs.
242 According to our model, the duration of the co-pairing period, the relative time between the cholinergic and
243 glutamatergic inputs, as well as their frequency during the co-pairing period, can modulate the efficiency and direction
244 of plasticity. Results of our simulations show that the longer the co-pairing period, the longer will be the transient
245 duration, where the potentiation transient duration was defined as the time it takes the EPSCs to return to its
246 baseline value once the co-pairing period is over (Figure 3A). We observe a positive relationship between the
247 frequency of the glutamatergic and cholinergic inputs during a fixed period of paring protocol, and the duration of the
248 potentiation transient (Figure 3 B). Interestingly, our simulations suggested that while changing the co-pairing
249 period and the frequency of stimulation modulates the efficiency of the induction of potentiation, it does not
250 change the direction of plasticity. It was only when varying the relative time between the ACh and glutamate
251 pulses that we could induce a change in the direction of the plasticity. For the pairing of single pulses, if the
252 glutamatergic inputs arrive to I and E_D within $0.7 < \Delta t < 20.2$ msec following the ACh pulse potentiation will be
253 induced. If $20.2 < \Delta t < 38$ msec, depression is induced (Figure 3C). If instead of single pulses we pair doublets of
254 glutamate and ACh, the potentiation and depression window change. The potentiation window is of $0.3 < \Delta t <$
255 18.27 msec, while the depression window is $-6.28 < \Delta t < 0.3$ msec and $18.27 < \Delta t < 70$ msec (see Figure 3D and
256 S1).
257
258 [Figure 3]
259

260 **Disinhibition of the CA1 pyramidal cell dendritic compartment enables potentiation of the SC-CA1**
261 **synaptic transmission.**

262 As we have shown in Figure 2, our model shows a decrease in GABA release from I-cells during the co-pairing period.
263 Based on this result, we hypothesize that a decrease of GABAergic inhibition of E_D allows for the potentiation of the
264 SC-evoked EPSC of the pyramidal cell dendritic compartment. To study the role of disinhibition of E_D in the
265 potentiation of the SC-CA1 excitatory synapse, we use a model where E_D receives a pulse of glutamate followed by a
266 pulse of GABA, except during a disinhibition period when it only receives pulses of glutamate. We also paired, *in vitro*,
267 inhibition of Sst interneurons with SC stimulation.

268 From Figure S2 we see that the rise and decay time of GABA concentration release that results from
269 the spiking of the I-cells is almost instantaneous. Therefore for simplification, in this section GABA is
270 modelled as a square pulse. Both glutamate and GABA release pulses are modeled as square pulses with a duration
271 of 1 msec and 1 mM of amplitude. E_D receives one pulse of glutamate per minute, followed by a pulse of GABA
272 2 msec after, except during a disinhibition period when it only receives pulses of glutamate. We note that this
273 choice of simulated stimulation and pairing directly follows from the experimental protocol (see
274 Methods). We use such a model to study how can disinhibition of E_D modulate the induction of synaptic plasticity.

275 It was observed that during the disinhibition period the EPSC amplitude increases, and that the longer the
276 disinhibition period last, the longer these changes last. Specifically, our model shows that for a disinhibition period of
277 4 minutes, the EPSC returns to baseline once the disinhibition period is over, and that for a longer disinhibition period
278 of 8 minutes, the EPSC remains potentiated long after the disinhibition period is over (Figure 4D). This is in accordance
279 with experimental results, where inhibition of Sst interneurons projecting to CA1 pyramidal cells was paired with SC
280 stimulation for a short and long period of time (Figure 4C). Inhibition of Sst interneurons via eNpHR resulted in
281 increased SC-CA1 EPSC amplitude not only during the Sst inhibition, but also after the end of Sst inhibition. The EPSC
282 enhancement after the end of Sst inhibition lasted about 10min after 4 times of Sst inhibition and more than 30 min
283 after 8 times of Sst inhibition.

284

285 [Figure 4]

286

287 Given that the amplitude of the AMPA current is much larger than the NMDA current (a glutamate pulse with a
288 duration of 1 msec and 1 mM of amplitude elicits an AMPA current with an amplitude of 17.65 μA/cm^2 and a NMDA
289 current with an amplitude of 2.19 μA/cm^2), the AMPAR arethe greatest contributor for the EPSC of E_D. Therefore,
290 we deduce that the changes in the EPSC amplitude seen during the disinhibition period reflect changes in the
291 AMPARs maximal conductance, $\bar{g}_{\mathrm{AMPA}}$. In fact, AMPARs have been known to play an important role in the
292 regulation and expression of synaptic plasticity in the hippocampus (Barria, Muller, Derkach, Griffith, &
293 Soderling, 1997). From Figure 5 we see that there is an increase of $\bar{g}_{\mathrm{AMPA}}$ during the disinhibition period. The longer
294 the disinhibition period, the higher is the value of $\bar{g}_{\mathrm{AMPA}}$ when the disinhibition period is over. For a disinhibition period
295 of 4 minutes (blue line), there is an increase of $\bar{g}_{\mathrm{AMPA}}$ from 0.3 to 1.8 *mS/cm*^{2} during disinhibition. Afterwards, $\bar{g}_{\mathrm{AMPA}}$
296 gradually goes back to its baseline value. For a disinhibition period of 8 minutes (orange line), $\bar{g}_{\mathrm{AMPA}}$ increases from
297 0.3 to 2.8 *mS/cm*^{2}. When the disinhibition period is over, $\bar{g}_{\mathrm{AMPA}}$ remains potentiated.

298

299 [Figure 5]

300

301 In our simulations we saw hints that not only the maximal voltage-dependent calcium concentration crossing the
302 potentiation threshold set in the model, but also the dynamics of calcium are determinant for the synaptic plasticity.
303 Hence, we examined the dynamics of the intracellular calcium concentration to understand how it determines
304 disinhibition-driven synaptic plasticity. From Figures 5C and D we see that calcium concentration increases
305 significantly during the disinhibition period, crossing the potentiation threshold Θ_p with a significant margin. For both
306 the short and long disinhibition, after the end of the disinhibition period, the calcium levels decrease, yet they remain
307 above Θ_p. This clearly shows that the maximal calcium concentration, Ca_{max}, is not the sole determinant of long-
308 term synaptic potentiation. In the case of a short disinhibition period, each pairing of GABA and glutamate after the
309 disinhibition period will elicit a calcium pulse with a smaller amplitude than the previous one. Eventually, at t=25 min,
310 the calcium concentration that results from the pairing is not enough to cross the potentiation threshold, and by the
311 time t=30 min it does not cross either the potentiation or the depression threshold, having a similar amplitude as
312 before the disinhibition period. In the case of a long disinhibition period, each pairing performed after the

disinhibition period evokes a calcium pulse with the same amplitude. To better visualize the synaptic and calcium dynamics immediately after the disinhibition period in both cases, we plot the system's trajectory in the Ca-$\bar{g}_{AMPA}$ plane. We do so for $\bar{g}_{AMPA}(t_{init})$=1.8 mS/cm^2 and for $\bar{g}_{AMPA}(t_{init})$=2.8 mS/cm^2 (Figure 5E), which are the values of $\bar{g}_{AMPA}$ at the end of the disinhibition period for the short- and long- disinhibition durations. For $\bar{g}_{AMPA}(t_{init})$=1.8 mS/cm^2, the calcium concentration crosses the potentiation threshold Θ_p (Ca_{max} = 1.62 mM) but there is a total decrease in $\bar{g}_{AMPA}$. For $\bar{g}_{AMPA}(t_{init})$=2.8 mS/cm^2, the calcium concentration crosses Θ_p to a larger extent (Ca_{max} = 1.72 mM) and there is a total increase of $\bar{g}_{AMPA}$. This result reveals the importance of calcium dynamics in the induction of plasticity. Changing the calcium dynamics, for example by changing the decay constant of calcium, will change the outcome of plasticity induction by changing the time calcium spends just above the potentiation threshold – when potentiation is induced – and between the depression and potentiation threshold – when depression is induced (see Fig. S4).

These results also suggest that it is not sufficient for calcium concentration to cross the potentiation threshold to result in a potentiation of $\bar{g}_{AMPA}$. To verify this, we looked at changes in maximal conductance of the postsynaptic AMPAR, $\Delta\bar{g}_{AMPA}$, as a function of the amplitude of the intracellular calcium, Ca_{max}. From Figure 5F we see that as Ca_{max} increases we only start to have potentiation ($\Delta\bar{g}_{AMPA} > 0$) when Ca_{max} crosses not the potentiation threshold Θ_p, but what we will call an effective potentiation threshold Θ^{eff}, at Ca_{max}=1.61 mM.

Based on our findings, we infer that the disinhibition period can govern the efficiency of the plasticity induction by controlling the extent to which $\bar{g}_{AMPA}$ is potentiated, which in turn will determine the outcome of the stimulation protocol after disinhibition period.

Similarly to what was done in the previous section, we wanted to examine how other parameters influence the plasticity of SC-CA1 EPSCs. According to our model, the amplitude of the GABA pulse, $GABA_{max}$, as well as the relative time between the glutamate and GABA pulses, $\Delta t_{(GABA\text{-}Glu)}$, can modulate plasticity. We also see that the regions of the $\Delta t_{GABA\text{-}Glu}$-$GABA_{max}$ parameter space that define the zones of depression and potentiation changes with the $\bar{g}_{AMPA}$ (Figure 6). Therefore, the same induction protocol may induce potentiation or depression, more or less efficiently, depending on the current state of phosphorylation of the AMPA receptors, i.e. $\bar{g}_{AMPA}$, and on the decrease of GABA during disinhibition.

[Figure 6]

340 **Membrane potential of CA1 pyramidal dendritic compartment controls direction of plasticity**

341 Based on our results, we hypothesize that the voltage of the pyramidal dendritic compartment V_{E_D} is the critical
342 variable in the model that controls the direction of plasticity. To explore this hypothesis, we will use phase-plane analysis.
343 To use this technique, we reduce our 6-variable model (V_{E_D}, $\bar{g}_{AMPA}$, r_N, r_G, r_{AMPA}, Ca) to its slow 2-variable subsystem
344 ($\bar{g}_{AMPA}$, r_N) so that it may be represented graphically and understood entirely by doing phase-plane analysis. We do
345 this by exploring the time scale differences between the dynamical variables of the system. The maximal conductance
346 of the AMPAR and the fraction of open NMDA receptor channels, $\bar{g}_{AMPA}$ and r_N, are significantly slower than the other
347 variables. We use a quasi-equilibrium approximation to the fast variables Ca, r_{AMPA} and r_G, i.e. we replace this
348 variables by their steady state value, to obtain a reduced 2-variable $\bar{g}_{AMPA}$–r_N with V_{E_D} as a parameter. We then plot
349 the trajectories and respective nullclines of the reduced system in the $\bar{g}_{AMPA}$–r_N plane for 2 different values of V_{E_D}, V_{E_D}
350 = -69 mV and V_{E_D} = -60 mV (Figure 7). In the reduced r_N–$\bar{g}_{AMPA}$ system, r_N is the fast variable, while $\bar{g}_{AMPA}$ is the slow
351 variable. We note that from the dynamical systems theory we know that in such fast-slow systems, the solutions
352 tend to move rapidly towards (or away from) the fast variable nullclines, and then flow slowly along it (the so-called
353 slow manifold). Hence for most of the time, the dynamics of the system are functionally governed by the shape and
354 the location of the fast nullcline relative to the slow one and the slow-variable flow along it. More precisely, starting
355 from some general initial condition, the system will be governed by the fast subsystem r_N until it reaches its steady
356 state $\frac{dr_N}{dt} = 0$. The system will then evolve slowly governed by the slow subsystem $\bar{g}_{AMPA}$. As shown in Figure 7, the
357 parameter V_{E_D} controls the nullcline of $\bar{g}_{AMPA}$. For V_{E_D} = −69 mV, the nullcline of r_N is below the one of $\bar{g}_{AMPA}$. Therefore,
358 when the steady state of r_N is reached, the system will be driven to the left, which corresponds to a decrease in
359 $\bar{g}_{AMPA}$ - or, in other words, to depression. On the other hand, when V_{E_D} is increased to −60 mV the nullcline of r_N is
360 now located above $\bar{g}_{AMPA}$, and the system will evolve towards the right once the steady state of r_N is reached - we
361 have potentiation.

362

363 [Figure 7]

364

365 These results suggest that a necessary condition for the induction of synaptic plasticity is the depolarization of the

366 pyramidal cell membrane, which can be accomplished by pairing the activation of the SC with the disinhibition.

367

368 **Model Predictions:**

369 Results of model simulations and analysis make several testable predictions. Despite not knowing the exact type of
370 s.o. interneuron that is providing feedforward inhibition to the CA1 pyramidal cell, our model predicts that it should
371 be an interneuron with fast dynamics, i.e. with dynamics comparable to the one of the pyramidal cells.

372 In this work (both in modelling and experimentally), activation of OLM cells is accomplished through cholinergic
373 activation of α7 nAChRs. In our model, α7 receptor activation provides a depolarising current to the OLM neurons.
374 Therefore, we expect that activation of the OLMα2 interneurons through any mechanism other than septal
375 cholinergic activation, for example through optogenetic stimulation, would lead to the similar results.

376 Finally, our model predicts a relationship between the relative timing of the septal and hippocampal stimulus paring
377 and the direction of the synaptic plasticity at the SC-PYR synapse. According to our simulations, increasing the
378 frequency of septal and hippocampal paired stimulation can induce plasticity more easily, i.e. less pairings would be
379 required to induce LTP. At the same time, we predict that increasing the relative time between septal and
380 hippocampal activation can induce LTD instead of LTP.

381

382

383 ## Discussion

384 This work set out to explain how cholinergic activation of hippocampal OLM interneurons paired with hippocampal
385 stimulation can potentiate CA1 pyramidal cell EPSC responses. Our modelling results suggest that co-pairing
386 cholinergic activation of OLM interneurons results in the disinhibition of CA1 pyramidal cells, which paired with
387 hippocampal stimulation potentiates CA1 pyramidal cell SC-evoked EPSCs. We also show general proof of principle
388 of how synaptic plasticity is controlled by the disinhibition of the postsynaptic pyramidal membrane through a
389 disynaptic GABA-ergic circuit.

390 OLM cells are a major class of GABAergic interneurons located in the stratum oriens hippocampal layer that inhibit
391 pyramidal cells dendritic compartment located in the stratum lacunusom-moleculare layer, reducing the strength of

392 EC inputs. However, there are recent findings showing that activation of these cells can facilitate LTP in SC-CA1
393 pathway, likely by inhibiting s.r. interneurons that synapse on the same dendritic compartment as the SC,
394 counteracting SC feedforward inhibition (Leão, et al., 2012).
395 We found that repeated pairing of cholinergic inputs with hippocampal stimulation can induce plasticity if the inputs
396 are tightly timed. The time window for potentiation depends greatly on the dynamics of the O-cells, I-cells and the
397 calcium dynamics. This is in accordance with experimental findings showing that activation of cholinergic inputs to the
398 hippocampus can directly induce different forms of synaptic plasticity depending on the input context in the hippocampus, with
399 a timing precision in the millisecond range (Gu & Yakel, Timing-dependent septal cholinergic induction of dynamic hippocampal
400 synaptic plasticity, 2011). Our model also shows that the longer the co-pairing period and the higher the frequency of
401 stimulation during the co-pairing period, the longer lasting is the potentiation of the synapse.
402 It is important to note that in our model, the OLM fast-spiking interneuron and pyramidal cell are connected through
403 a feedforward connection. It is likely that recurrent connections between these neurons exist. However, adding these
404 recurrent connections to our model does not qualitatively change our results, provided we adjust the parameters
405 corresponding to the potentiation and depression threshold, Θ_p and Θ_d, and/or the potentiation and depression
406 amplitudes, $\gamma_p$and γ_d, as well as the maximal conductance of the synaptic currents.
407 According to our model, the key mechanism behind paired cholinergic induction of synaptic plasticity is the
408 disinhibition of the pyramidal cell dendritic compartment. Cholinergic activation of the O-cell inhibits the fast-spiking
409 I-cell that projects to the dendritic compartment E_D. The disinhibition of E_D paired with glutamatergic stimulation
410 allows for the depolarization of the pyramidal dendritic compartment. This leads to increased NMDAR activation and
411 intracellular calcium concentration sufficient to upregulate postsynaptic AMPAR permeability and potentiate the
412 excitatory synapse. It is worth mentioning that we consider a minimal model and that there are other pathways that
413 may play a role in the induction of plasticity by modulating the calcium dynamics at the s.r. dendritic compartment;
414 namely, the OLM projection to the distal dendrites of the CA1 pyramidal neurons.
415 In order to study in greater detail the mechanisms behind the induction of plasticity through disinhibition, we
416 modelled changes in synaptic strength when glutamatergic activation of E_D is paired with locally reduced GABA.
417 Before the disinhibition period starts, the cell receives both excitatory and inhibitory inputs. An excitatory input
418 evokes an EPSP mediated by AMPAR. The EPSP is followed by a $GABA_A$-mediated IPSP. Because of slow kinetics and

419 voltage-dependence, at that time, the NMDAR receptors are not in the open state and there is no influx of calcium.
420 During the disinhibition period, the cell only receives the excitatory inputs (GABA inputs are suppressed). The
421 pyramidal cell membrane at (or sufficiently near to) the glutamatergic synapse is able to depolarize enough to relieve
422 the Mg^{2+} block from the NMDA receptors, allowing calcium to permeate through the receptor channel (Figure 8).
423 Therefore, during the disinhibition period, every time the pyramidal cell receives a pulse of glutamate, the
424 intracellular calcium concentration crosses the potentiation threshold Θ_p, and $\bar{g}_{\mathrm{AMPA}}$ increases.
425
426 [Figure 8]
427

428 Therefore, down-regulation of the GABAergic signaling during disinhibition leads to increased NMDAR activation.
429 Because of the receptor's high calcium permeability, there is an elevation in intracellular calcium concentration large
430 enough to initiate molecular mechanisms that result in the insertion/phosphorylation of the AMPAR. In our model,
431 this translates into an increase in the AMPAR maximal conductance $\bar{g}_{\mathrm{AMPA}}$. Moderate calcium concentrations, on the
432 other hand, result in the removal of AMPARs. Because changes in calcium concentration are not instantaneous, the
433 potentiation/depression of the synapse is a result of a balance between the insertion/removal of AMPARs during the
434 period in which Ca concentration is above potentiation/depression threshold. During disinhibition, this balance is
435 positive and there is a total increase in $\bar{g}_{\mathrm{AMPA}}$. The more times we pair disinhibition with SC stimulation, i.e. the longer
436 the disinhibition period, the higher will be the value of $\bar{g}_{\mathrm{AMPA}}$ by the end of the disinhibition period. After the
437 disinhibition period, if the increase of $\bar{g}_{\mathrm{AMPA}}$ was large enough, the calcium resultant from glutamatergic and
438 GABAergic stimulation is such that there was a balance between potentiation and depression, which is close to zero
439 ($\Delta\bar{g}_{\mathrm{AMPA}}$=-0.0002). Therefore, the synapse remains potentiated long after the disinhibition period is over. If there is
440 no stimulation after the disinhibition period, $\bar{g}_{\mathrm{AMPA}}$ slowly decays to its initial value (i.e. its value before the disinhibition
441 period). If the increase of the AMPAR permeability is high enough, the potentiation of the excitatory synapse is
442 maintained when the disinhibition period is over through repeated stimulation of the SC that keeps a balance between
443 the down and upregulation of the AMPARs. This is in accordance with experimental results that show that repeated
444 pairing of inhibition of Sst interneurons (which are not OLM interneurons) that target the CA1 pyramidal cell with SC

445 stimulation can induce plasticity.

446 Our model is robust to changes of parameters that maintain the same ratio of potentiation/depression. Meaning
447 that, for example, for different values of the potentiation amplitude γ_p, there is (at least) a pair of maximal depression
448 γ_d and decay constant σ for which our results remain the same (Fig. S3).

449 It is worth noting that the type of synaptic plasticity induced depends on the value of maximal conductance of the
450 postsynaptic AMPAR, $\bar{g}_{\mathrm{AMPA}}$, as shown in Figure 6. Therefore, despite not having explicit memory or considering
451 metaplasticity, our model shows that future changes in synaptic strength depend on previous plasticity events and
452 how these changed $\bar{g}_{\mathrm{AMPA}}$. This explains why, after the disinhibition period, pairs of glutamate and GABA pulses with
453 the same characteristics are going to induce different results when the disinhibition period was short or long.

454 In summary, using our minimal biophysically-based model, we accounted for key experimental observations that
455 provided a cogent explanation for the role of the septal cholinergic pathway activation in the induction of
456 hippocampal synaptic plasticity. Our modeling work suggests that GABAergic neurotransmission controls the local
457 pyramidal voltage in the vicinity of the glutamatergic synapses, thereby the inhibitory synapses critically modulate
458 excitatory transmission and the induction of plasticity at excitatory synapses. This puts into evidence the importance
459 of dendritic GABA and glutamate co-location in shaping local plasticity rules. Our work also suggests a cholinergic
460 mechanism for the inhibition of GABA release at the pyramidal dendrites and consequent potentiation of excitatory
461 synapses, unraveling the intricate interplay of the hierarchal inhibitory circuitry and cholinergic neuromodulation as a
462 mechanism for hippocampal plasticity.

463 Previous work by Gu et al. (2017) showed that co-paired activation of the cholinergic input pathway from the septum
464 to the hippocampus, either electrically or using optogenetics, with stimulation of the Schaffer collateral pathway
465 could readily induce theta oscillations in a co-culture septal-hippocampal-entorhinal preparation. They also observed
466 that performing this co-pairing mechanism increased excitatory transmission in the hippocampus and subsequent
467 outputs to the EC in slice co-cultures. Moreover, after synaptic plasticity has been induced it becomes easier to evoke
468 the theta rhythm in the preparation (one pulse stimulus of the SC is sufficient to generate theta oscillations in the
469 circuit with the same characteristics as before) (Gu & Yakel, Inducing theta oscillations in the entorhinal hippocampal
470 network in vitro, 2017; Gu, Alexander, Dudek, & Yakel, 2017). Therefore, induction of hippocampal plasticity, in
471 particular potentiation of the CA1 EPSPs, appears to facilitate the generation of the theta rhythm. Moreover, a recent

472 study directly linked OLMα2 interneurons to theta oscillations (Mikulovic, et al., 2018). We thus may speculate that the
473 action of ACh on the α7 nAChRs at the OLMα2 neurons potentiates the SC-CA1 synapses to close the critical link in the
474 synaptic chain of events, enabling recurrent reverberation of excitation in the hippocampal-entorhinal theta generating
475 circuit. Understanding the mechanisms underlying the induction of hippocampal plasticity by this co-pairing
476 mechanism will allow future studies of how changes on the synaptic level can propagate to the network level and
477 change the mechanisms of theta generation.
478 We may also note that our results can be relevant to understanding the neural circuit origins of pathological conditions.
479 The hippocampus is one of the earliest brain structures to develop neurodegenerative changes in Alzheimer's disease
480 (AD) (Arriagada, Growdon, Hedley-Whyte, & Hyman, 1992). Numerous studies suggest that cognitive deficits in AD such
481 as memory impairment are caused in part by cholinergic dysfunction action on hippocampal GABAergic interneurons
482 (Schmid, et al., 2016; Haam & Yakel, 2017). Here, we have shown that a decrease in the conductance of cholinergic α7
483 nAChRs on OLM interneurons caused the impairment of induction of hippocampal synaptic plasticity.
484
485

486 **Acknowledgments**

487 This research was supported by the Intramural Research Program of the NIH, National Institute of Environmental
488 Health Sciences. IG and BSG acknowledge support from the Fondation pour la Recherche sur Alzheimer, CNRS,
489 INSERM, ANR-17-EURE-0017 and ANR-10-IDEX-0001-02 . BSG acknowledges funding from HSE Basic
490 Research Program and the Russian Academic Excellence Project "5-100."
491
492

493 **References**

494 Arriagada, P., Growdon, J., Hedley-Whyte, E., & Hyman, B. (1992). Neurofibrillary tangles but not senile plaques
495 parallel duration and severity of Alzheimer's disease. *Neurology, 42*(3.1), 631-639.
496 Barria, A., Muller, D., Derkach, V., Griffith, L., & Soderling, T. (1997). Regulatory Phosphorylation of AMPA-type
497 Glutamate receptors by CaM-KII during long-term potentiation. *Science, 276*(5321), 2042-2045.
498 Bliss, T. (1973). Long-lasting potentiation of synaptic transmission in the dentate area of the anaesthetized rabbit

following simulation of the perforant path. *The Journal of Physiolopgy, 232*(2), 331-356.

Chevalerye, V., & Piskorowski, R. (2014). Modulating excitation through plasticity at inhibitory synapses. *Frontiers in Cellular Neuroscience, 8*.

Chevaleyre, V., & Piskorowski, R. (2014). Modulating excitation through plasticity at inhibitory synapses. *Frontiers in Cellular Neuroscience, 8*.

Collingridge, G., Kehl, S., & McLennan, H. (1983). Excitatory amino acids in synaptic transmission in the Schaffer Collateral-commissural pathway of the rat hippocampus. *The Journal of Physiology, 334*(1), 33-46.

Destexhe, A., Mainen, Z., & Sejnowski, T. (1998). Kinetic models of synaptic transmission. In C. Koch, & I. Segev, *Methods in neuronal modeling: from ions to networks.* The MIT Press.

Graupner, M., & Gutkin, B. (2013). Endogenous cholinergic inputs and local circuit mechanisms govern the phasic mesolimbic dopamine response to nicotine. *PLOS Computational Biology, 9*(8).

Griguoli, M., & Cherubini, E. (2012). Regulation of hippocampal inhibitory circuits by nicotinic acetylcholine receptors: nAChRs and inhibitory circuits in the hippocampus. *The Journal of Physiology, 590*(4), 655-666.

Gu, Z., & Yakel, J. (2011). Timing-dependent septal cholinergic induction of dynamic hippocampal synaptic plasticity. *Neuron, 71*(1), 155-165.

Gu, Z., & Yakel, J. (2017). Inducing theta oscillations in the entorhinal hippocampal network in vitro. *Brain Structure and Function, 222*(2), 943-955.

Gu, Z., Alexander, G., Dudek, S., & Yakel, J. (2017). Hippocampus and Entorhinal Cortex recruit cholinergic and NMDA receptors separately to generate hippocampal theta oscillations. *Cell Reports, 21*(12), 3585-3595.

Gu, Z., Smith, K., Alexander, G., Guerreiro, I., Dudek, S., Gutkin, B., . . . Yakel, J. (2020). Hippocampal interneuronal a7 nAChRs modulate theta oscillations in freely moving mice. *Cell Reports, 31*(10), 107740.

Haam, J., & Yakel, J. (2017). Cholinergic modulation of the hippocampal region and memory function. *Journal of Neurochemistry, 142*, 111-121.

Hodgkin, A., & Huxley, A. (1952). A quantitative description of membrane current and its application to conduction and excitation in nerve. *The Journal of Physiology, 117*(4), 500-544.

Lüscher, C., & Malenka, R. (1994). Synaptic plasticity in the hippocampus: LTP and LTD. *Cell, 78*(4), 535-538.

Leão, R., Mikulovic, S., Leão, K., Munguba, H., Gezeluis, H., Enjin, A., . . . Kullander, K. (2012). OLM interneurons

526 differentially modulate CA3 and entorhinal inputs to hippocampal CA1 neurons. *Nature Neuroscience,*
527 *15*(11), 1524-1530.
528 Levin, E. (2002). Nicotinic receptor subtypes and cognitive function. *Journal of Neurobiology, 53*(4), 633-640.
529 Mikulovic, S., Restrepo, C., Siwani, S., Bauer, P., Pupe, S., Tort, A., . . . Leao , R. (2018). Ventral hippocampal OLM
530 cells control type 2 theta oscillations and response to predator odor. *Nature Communications, 9*(1), 3638.
531 Rotstein, H., Pervouchine, D., Acker, C., Gillies, M., White, J., Buhl, E., . . . Kopell, N. (2005). Slow and fast inhibition
532 and h-current interact to create a theta rhythm in a model of CA1 interneuron network. *Journal of*
533 *Neurophysiology, 94*, 1509-1518.
534 Saudargiene, A., & Graham, B. (2015). Inhibitory control of site-specific synaptic plasticity in a model CA1 pyramidal
535 neuron. *Biosystems, 130*, 37-50.
536 Schmid, L., Mittag , M., Poll, S., Schwarz, M., Remy, S., & Fuhrmann, M. (2016). Dysfunction of somatostatin-
537 positive interneurons associated with memory deficits in an Alzheimer's disease model. *Neuron, 92*(1),
538 114-125.
539 Shouval, H., Bear, M., & Cooper, L. (2002). A unified model of NMDA receptor-dependent bidirectional synaptic
540 plasticity. *Proceedings of the National Academy of Sciences, 99*(16), 10831-10836.
541 Wigstrom, H., & Gustafsson, B. (1985). Facilitation of hippocampal long-lasting potentiation by GABA antagonists.
542 *Acta Physiol. Scand., 125*, 159-172.
543 Yakel, J. (2012). Nicotinic ACh Receptors in the hippocampus: role in excitability and plasticity. *Nicotine & Tobacco*
544 *Research, 14*(11), 1249-1257.
545

Table 1: Parameters of pyramidal cell, OLM interneuron, and fast-spiking interneuron dynamics. All the parameter values and expressions here described were taken from (Rotstein, et al., 2005).

Parameter	**Value**
O-cells	
C_m	1 $\mu F/cm^2$
g_{leak}	0.5 mS/cm^2
E_{leak}	-65 mV
$\bar{g}_K$	11 mS/cm^2
E_K	-90 mV
$\bar{g}_{Na}$	52 mS/cm^2
E_{Na}	55 mV
$\bar{g}_p$	0.5 mS/cm^2
$\bar{g}_h$	1.45 mS/cm^2
E_h	-20 mV
I-cells	
C_m	1 $mu\ F/cm^2$
g_{leak}	0.1 mS/cm^2
E_{leak}	-66 mV
$\bar{g}_K$	80 mS/cm^2
E_K	-100 mV
$\bar{g}_{Na}$	100 mS/cm^2
E_{Na}	50 mV

Table 2: Parameter values of synaptic currents *AMPA*, *NMDA* and $GABA_A$. The parameter values were based on (Graupner & Gutkin, 2013) and (Destexhe, Mainen, & Sejnowski, 1998).

Parameter	Value
α_A	10 $ms^{-1}mM^{-1}$
β_A	0.3 ms^{-1}
$[Mg^{2+}]$	1 mM
α_N	0.75 $ms^{-1}mM^{-1}$
β_N	6.6 x 10^{-3} ms^{-1}
α_G	3.3 $ms^{-1}mM^{-1}$
β_G	0.1 ms^{-1}
$\bar{g}_{\alpha 7}$	4 mS/cm^2
EC_{50}	80 x 10^{-3} mM
$\tau_{r\alpha 7}$	5 ms
n	1.73

Table 3: Parameter values for synaptic plasticity. The values were adjusted from (Shouval, Bear, & Cooper, 2002) to obtain calcium level changes able to induce potentiation and depression in our simulations.

Parameter	Value
σ	0.003
P_1	30 *ms*
P_2	P_1 x 10^{-4}
P_3	11.4
P_4	1 *ms*
ϑ_p	1.4
ϑ_d	1
γ_p	0.143
γ_d	0.105
α	0.2
τ_{Ca}	5 *ms*

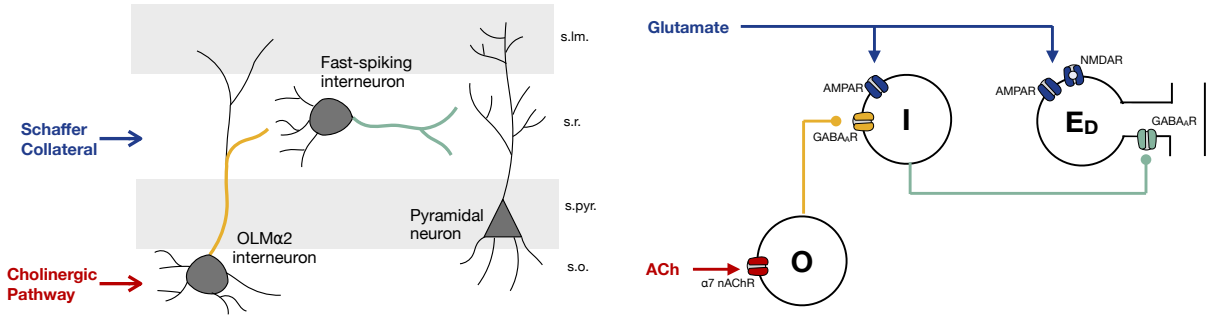

(A) **(B)**

Figure 1: Disynaptic disinhibition circuit for ACh induced long-term plasticity in the CA1. (A) Simplified wiring diagram of an interneuron network that mediates feedforward inhibition in the CA1 region of the hippocampus. Activation of the Schaffer Collateral (SC) pathway leads to the activation of CA1 pyramidal cell dendrites and of the stratum radiatum (s.r.) interneurons, which provide feedforward inhibition onto the pyramidal cell. Cholinergic activation of OLMα2 interneurons in stratum oriens (s.o.) leads to the inhibition of the s.r. interneurons, counteracting SC feedforward inhibition (Leão, et al., 2012). **(B)** Minimal network to investigate plasticity induced by pairing of cholinergic and SC activation. Glutamate activates postsynaptic AMPA and NMDARs at the pyramidal cell dendritic compartment E_D and postsynaptic AMPARs at I-cells, which in turn provide feedforward inhibition onto E_D by activating postsynaptic $GABA_A$Rs. Cholinergic inputs act on postsynaptic α7 nAChRs of O-cells, which results in GABA release of the O-cells that it is going to bind to postsynaptic $GABA_A$Rs of the I-cells.

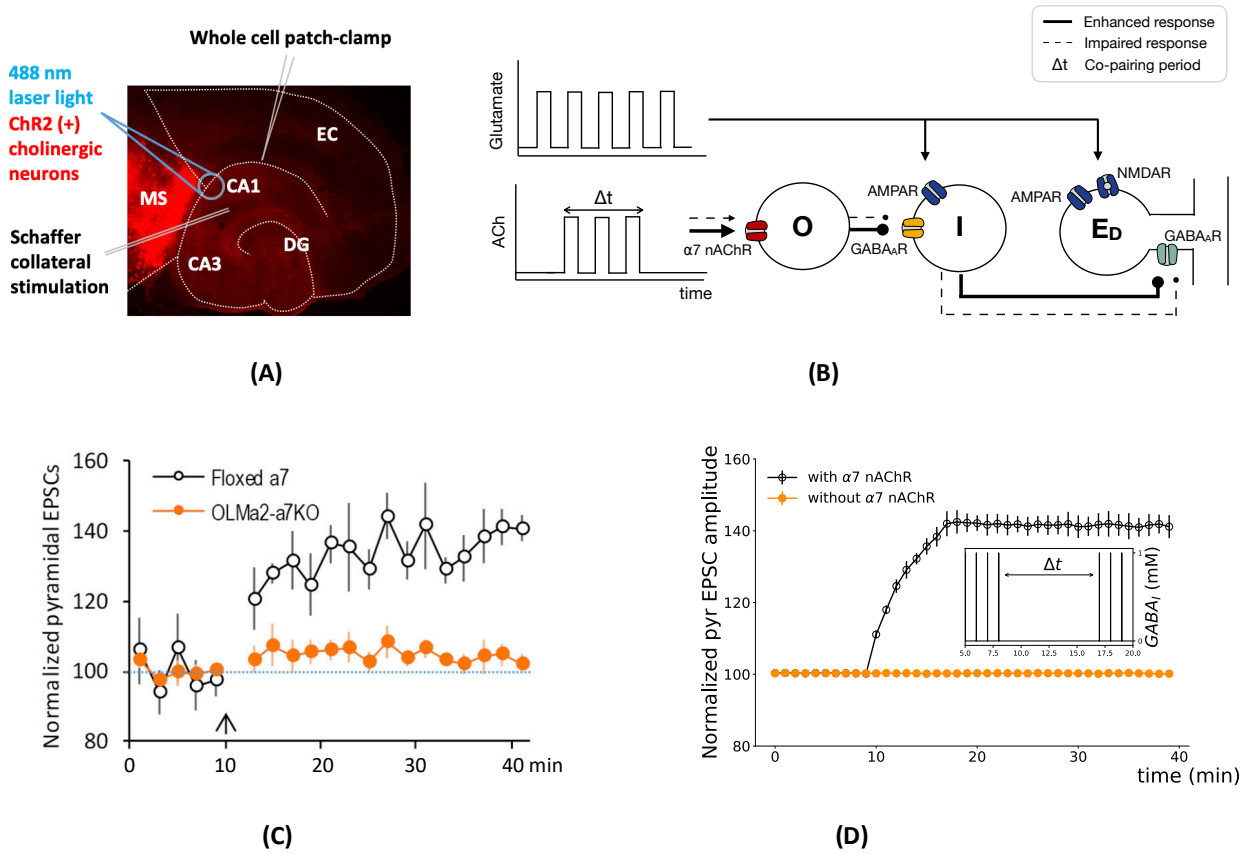

Figure 2: Cholinergic activation of OLM interneurons potentiates SC-evoked EPSCs. **(A)** Scheme of *in vitro* induction of cholinergic pairing induced hippocampal synaptic plasticity. EPSCs were recorded from CA1 pyramidal neurons. Cholinergic neurons were activated via channelrhodopsin-2 that was specifically expressed in ChAT-positive neurons. The Schaffer collateral (SC) pathway was activated by a stimulating electrode. Adapted from (Gu, Alexander, Dudek, & Yakel, 2017). **(B)** Scheme of minimal network used to study role of cholinergic inputs in the potentiation of SC-evoked EPSCs. Glutamatergic inputs activate the pyramidal cell dendritic compartment (E_D) and the fast-spiking interneuron (I) that projects to it. The OLM interneuron (O) is activated by ACh during the co-pairing period. **(C)** Normalized SC-evoked EPSC responses from CA1 pyramidal neurons showing that the enhancement of EPSCs was impaired in hippocampal slices from mice with selective α7 nAChR knockout in OLMα2 interneurons. Adapted from (Gu, Alexander, Dudek, & Yakel, 2017). **(D)** Numerical simulation of normalized EPSC amplitude when glutamatergic inputs acting on the I-cell and E_D are paired with cholinergic inputs acting on the O-cell. The EPSCs are calculated as the sum of postsynaptic AMPA and NMDA currents, I_{AMPA} and I_{NMDA}, and are a result of 10 simulations with white noise on the E_D membrane potential. Normalization of the results was calculated according with the expression (100 + (EPSC - EPSCmin).(150-100))/(EPSCmax - EPSCmin). Inset: Concentration of GABA released from fast-spiking interneurons (I), calculated according to equation 15 (see Methods).

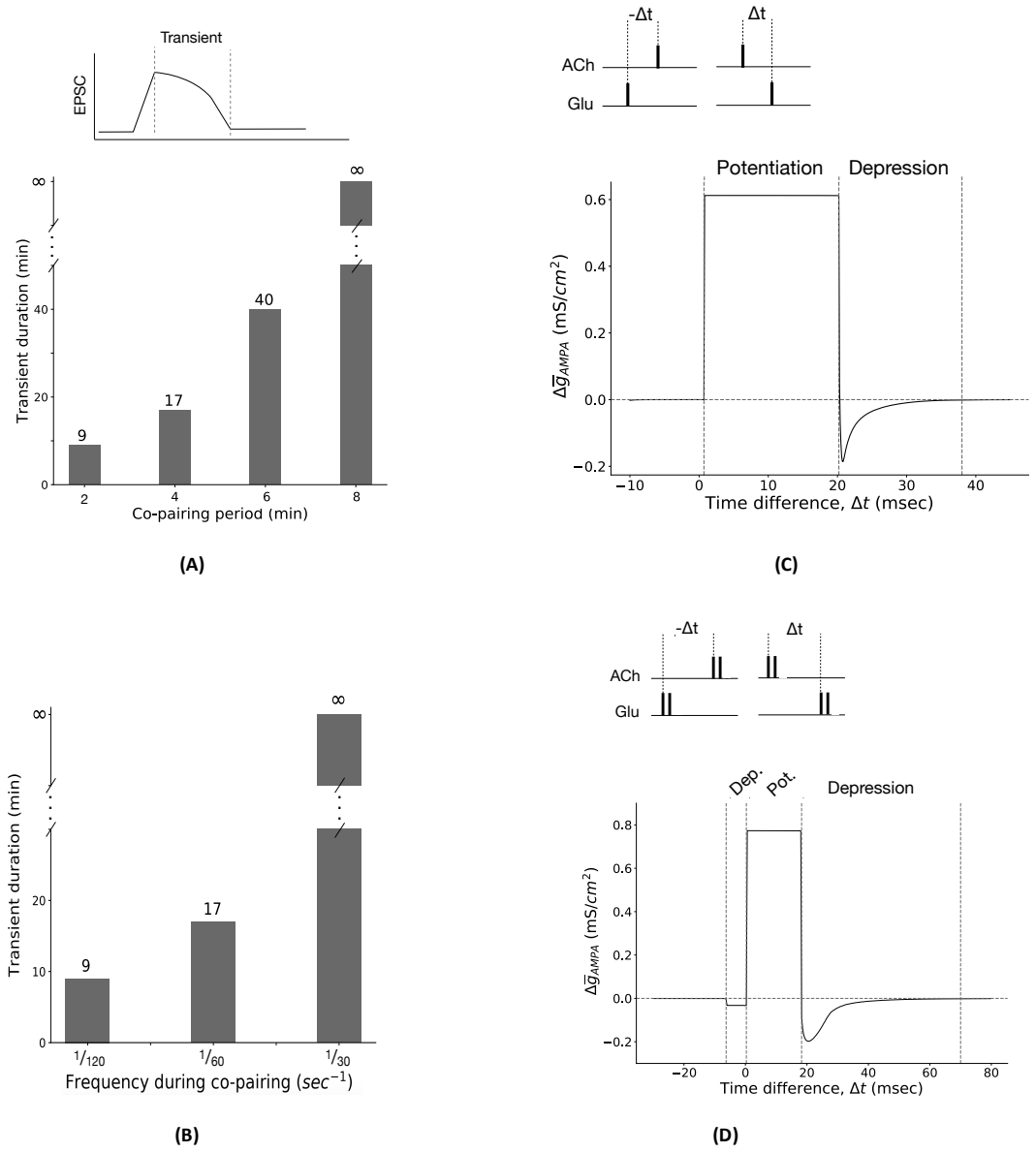

Figure 3: Co-pairing temporal parameters determine the duration and polarity of synaptic plasticity: relative timing between cholinergic and glutamatergic stimulation, extent of the co-pairing period, and the frequency of stimulation. (A) Synaptic strength transient duration is proportional to the extent of the pairing period. Here, the transient duration is defined as the time it takes the EPSC to go back to baseline after co-pairing is over. The I-cell and E_D receive a pulse of glutamate per minute. During the co-pairing period, the O-cell receives a pulse of ACh per minute, 1 msec prior to the pulses of glutamate. **(B)** Synaptic strength transient duration is proportional to the frequency of the

ACh and glutamate pulses during the co-pairing period. Before and after co-pairing period, the I-cell and E_D receive a pulse of glutamate per minute. During the co-pairing period (4 minutes), the frequency changes to $^1/_{120}$, $^1/_{60}$ or $^1/_{30}$ sec^{-1}, and the O-cell receives a pulse of ACh 1 msec prior to the pulses of glutamate with the same frequency. **(C)** Relative paring timing provides a window of opportunity for plasticity. If glutamatergic inputs are administrated within $0.7msec < \Delta t < 20.2msec$ the E_D excitatory synapse is potentiated. If glutamatergic inputs are administrated within $20.2msec < \Delta t < 38msec,$ depression is induced. Negative values of Δt correspond to glutamatergic stimulation prior to cholinergic activation. In that case, there are no changes in synaptic strength ($\Delta\bar{g}_{AMPA}$=0). The change in the AMPAR conductance $\Delta\bar{g}_{AMPA}$ is measured 60 msec after one pairing. **(D)** Pairing multiple pulses of glutamate and ACh can change window of opportunity for plasticity. Two pulses of glutamate and ACh with a frequency of $^1/_5$ $msec^{-1}$ are paired. If glutamatergic inputs arrive within $-6.28msec < \Delta t < 0.3msec$ or $18.27msec < \Delta t < 70msec$ of the cholinergic inputs, depression is induced. If glutamatergic inputs are administrated within $0.3 < \Delta t < 18.27$ msec, the E_D excitatory synapse is potentiated. The change in the AMPAR conductance $\Delta\bar{g}_{AMPA}$ is measured 60 msec after one pairing. Parameters for subfigure (D): g_N=0.18 mS/cm^2 and g_G=0.95 mS/cm^2 for the postsynaptic receptors of E_D. All other parameters are as indicated in the Methods.

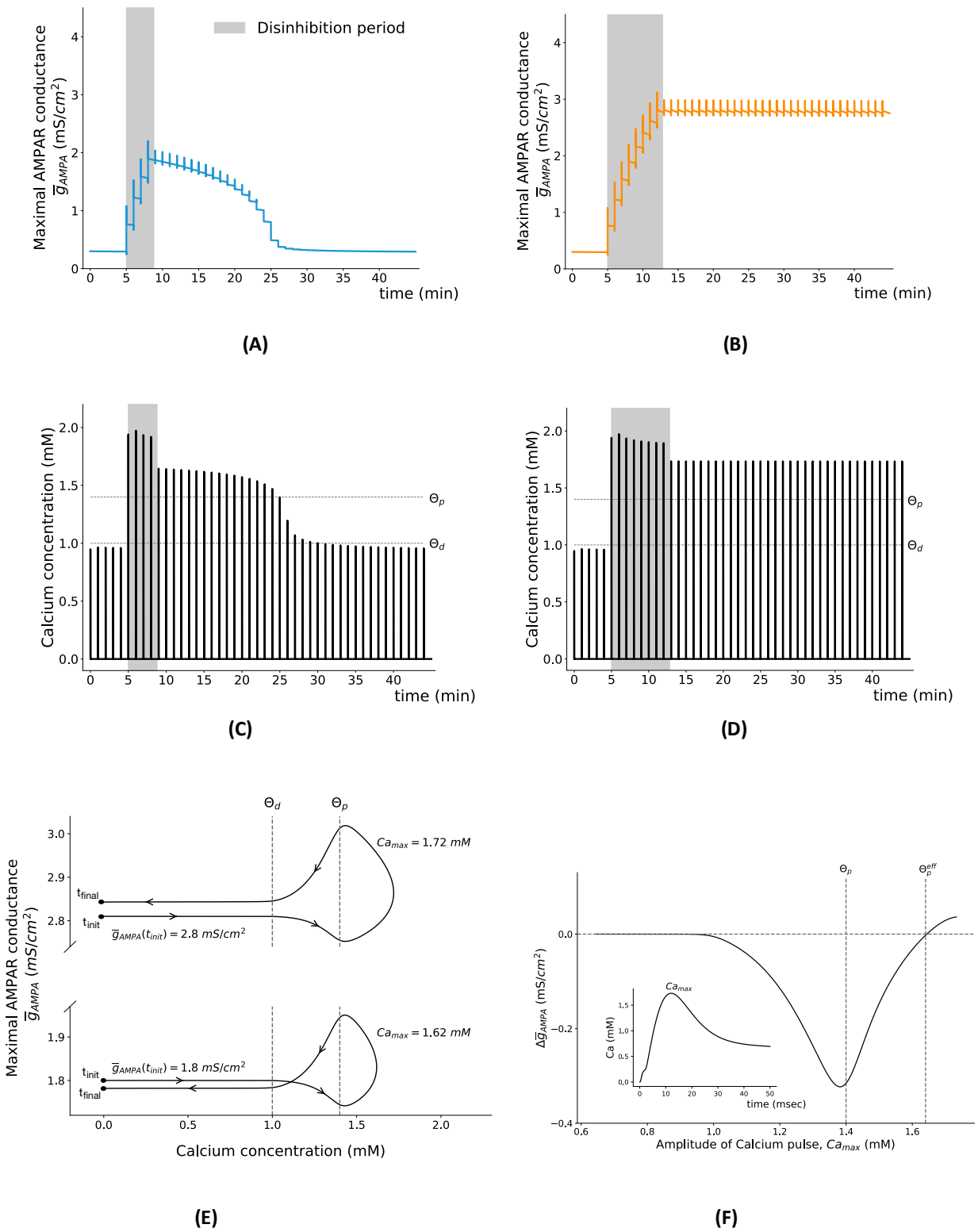

Figure 5: Calcium dynamic is key for the induction of synaptic plasticity. (A) Time course of maximal AMPAR

conductance, $\bar{g}_{\mathrm{AMPA}}$, when dendritic compartment is disinhibited for a short period of time (from t=5 min to t=9 min). The maximal AMPAR conductance increases from its initial value $\bar{g}_{\mathrm{AMPA}}$=0.3 mS/cm^2 to $\bar{g}_{\mathrm{AMPA}}$=1.8 mS/cm^2 during disinhibition period. **(B)** Time course of $\bar{g}_{\mathrm{AMPA}}$ when dendritic compartment is disinhibited for a long period of time (from t=5 min to t=13 min). It increases from its initial value $\bar{g}_{\mathrm{AMPA}}$= 0.3 mS/cm^2 to $\bar{g}_{\mathrm{AMPA}}$=2.8 mS/cm^2 during the disinhibition period. The AMPAR conductance $\bar{g}_{\mathrm{AMPA}}$ is described by equation 18. **(C)** Time course of intracellular calcium concentration when dendritic compartment E_D is disinhibited for a short period of time (from t=5 min to t=9 min). The pairing of a pulse of glutamate with a pulse of GABA at t=10 min, i.e. immediately after the disinhibition period, results in a calcium pulse with an amplitude of 1.62 mM. **(D)** Time course of intracellular calcium concentration when dendritic compartment is disinhibited for a long period of time (from t=5 min to t=13 min). The pairing of a pulse of glutamate with a pulse of GABA at t=14 min, i.e. immediately after disinhibition period, results in a calcium pulse with an amplitude of 1.72 mM. The calcium dynamics is described by equation 21 (see Methods). **(E)** Trajectories of the system in the $\bar{g}_{\mathrm{AMPA}}$-Ca plane when a pulse of glutamate is paired with a pulse of GABA for different initial values of $\bar{g}_{\mathrm{AMPA}}$. **(F)** Changes in the maximal AMPAR conductance, $\Delta\bar{g}_{\mathrm{AMPA}}$, as a function of the amplitude of intracellular calcium pulse, Ca_{max}. Each point of the graph was obtained by submitting E_D to a pulse of glutamate for different initial values of $\bar{g}_{\mathrm{AMPA}}$. This induced different levels of depolarization and, consequently, different levels of activation of NMDARs and calcium pulses of different amplitudes.

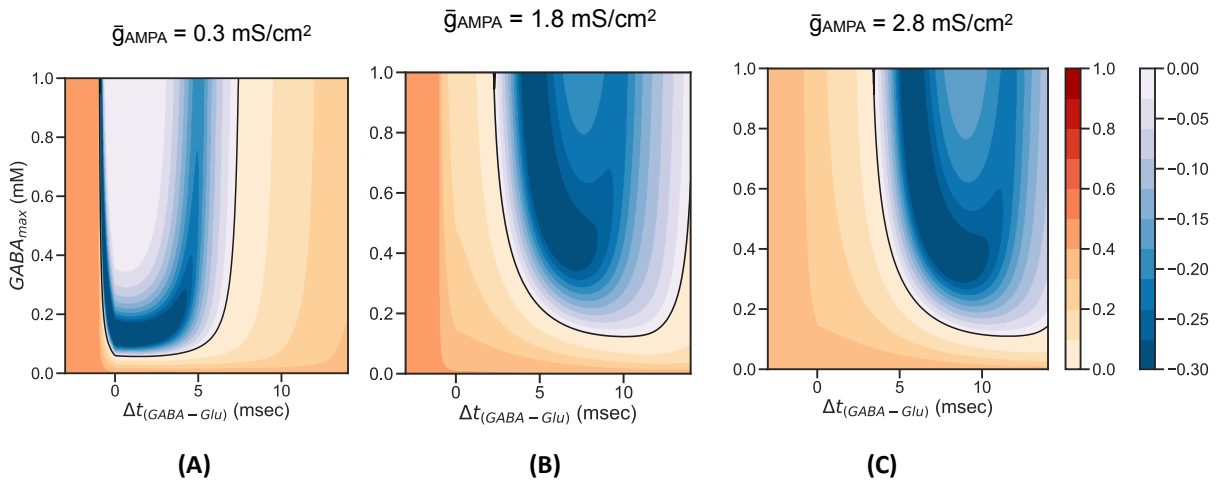

Figure 6: Amplitude of GABA pulse, $GABA_{max}$, and relative time between GABA and glutamate pulses, $\Delta t(GABA-Glu)$, control direction and efficiency of induction of synaptic plasticity. (a) Depression and potentiation regions for $\bar{g}_{AMPA}$= 0.3 mS/cm^2. **(b)** Depression and potentiation regions for $\bar{g}_{AMPA}$=1.8 mS/cm^2. **(c)** Depression and potentiation regions for $\bar{g}_{AMPA}$= 2.8 mS/cm^2.

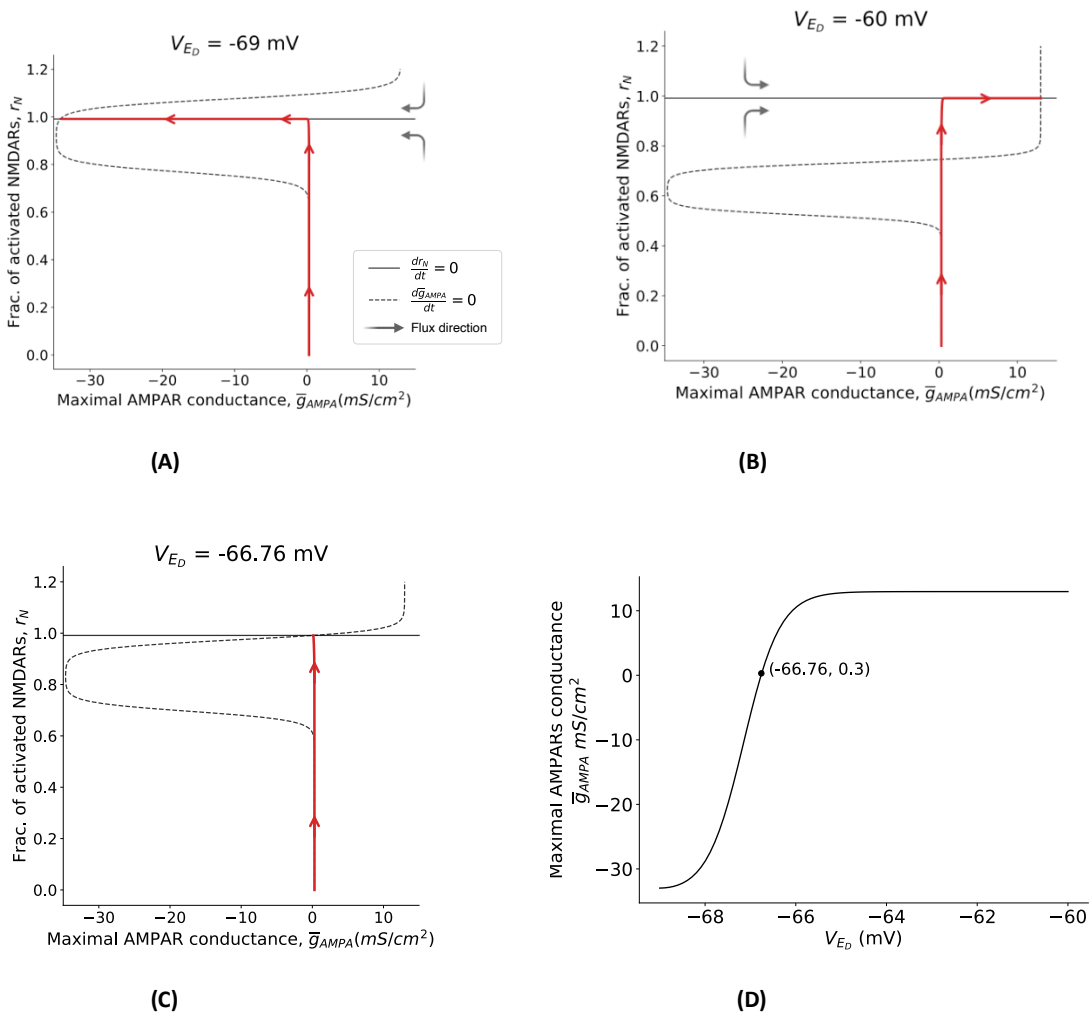

Figure 7: Trajectories of the slow subsystem r_N -$\bar{g}_{AMPA}$ for V_{ED} =-69 mV and V_{ED} =-60 mV, and respective nullclines. **(A)** For V_{ED} = −69 mV, the system has a stable fixed point at (-34.1,0.99). Initiating the system at $\bar{g}_{AMPA}$ = 0.3 mS/cm^2 and r_N =0, depression will be induced. **(B)** For V_{ED} = −60 mV, the system has a stable fixed point at (12.9,0.99). Initiating the system at $\bar{g}_{AMPA}$ = 0.3 mS/cm^2 and r_N =0, potentiation will be induced. **(C)** For V_{ED} = −66.76 mV, the system has a stable fixed point at (0.3, 0.99). Initiating the system at $\bar{g}_{AMPA}$ = 0.3 mS/cm^2 and r_N =0, no plasticity will be induced. **(D)** Bifurcation diagram for slow subsystem r_N-$\bar{g}_{AMPA}$. The system has a continuity of stable steady states. If we initialize the system with $\bar{g}_{AMPA}$ = 0.3 mS/cm^2, values of V_{ED} bellow -66.76 mV will move the system to a steady state with $\bar{g}_{AMPA}$ < 0.3 mS/cm^2, inducing depression. Values of V_{ED} above -66.76 mV will make the system evolve towards a steady state with $\bar{g}_{AMPA}$ > 0.3 mS/cm^2, inducing potentiation.

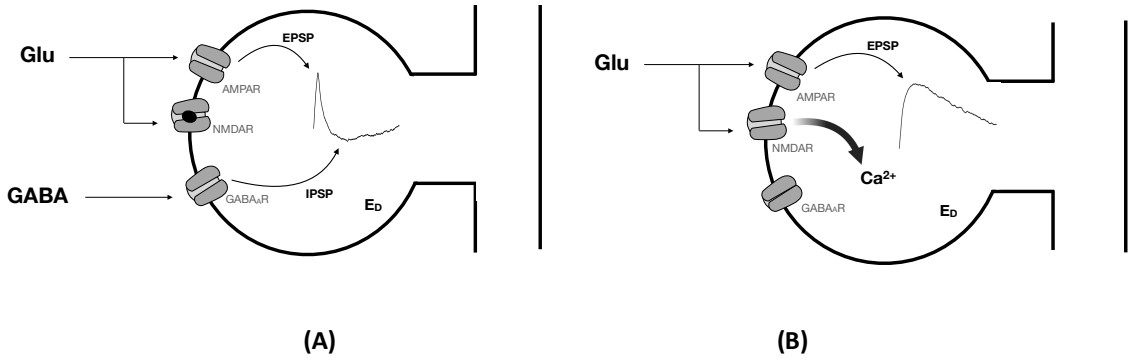

Figure 8: Scheme of the activation mechanisms of NMDARs and consequent calcium influx. **(A)** Glutamatergic activation evokes an EPSP mediated by AMPAR. The EPSP is followed by an IPSP mediated GABA acting on $GABA_A$ receptors. **(B)** Dendritic compartment does not receive GABAergic inhibition. The dendritic compartment is able to depolarize enough - and remain depolarized for long enough - to relieve Mg^{2+} block from NMDA receptors, allowing calcium to permeate through the receptor channel.

Supplementary Material

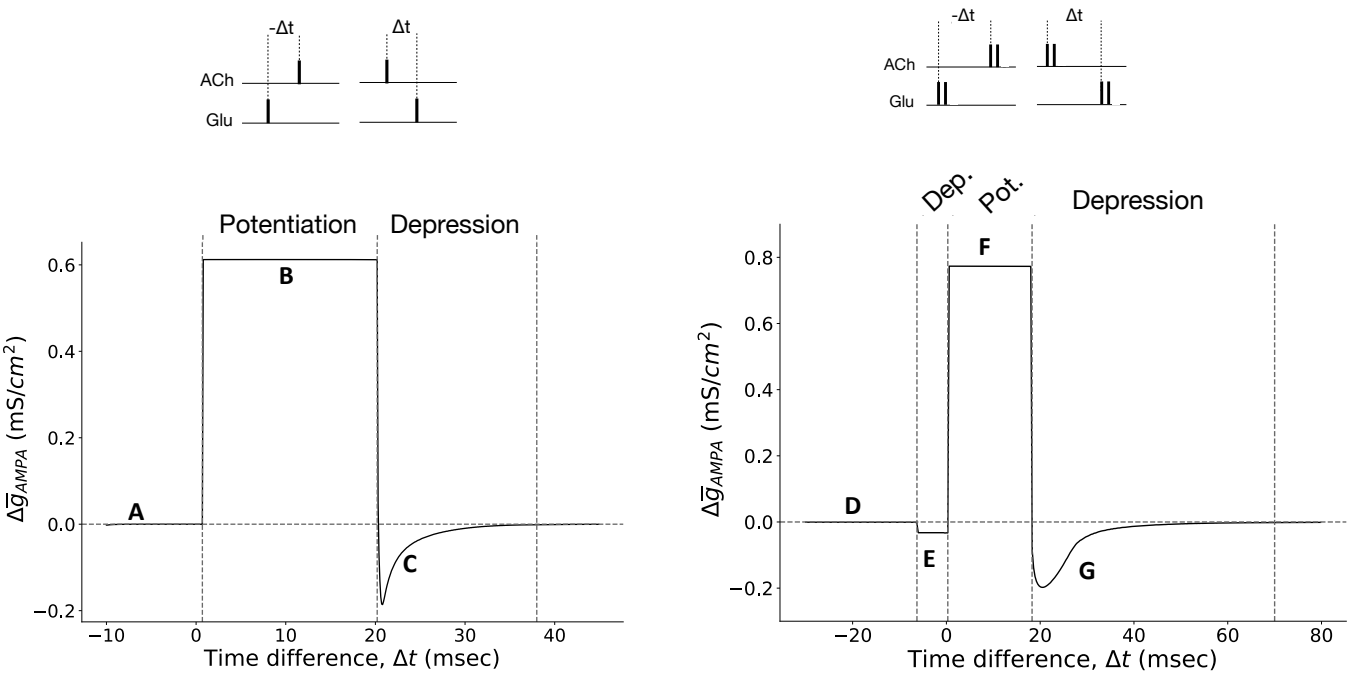

(A) **(B)**

Figure S1: (A) Single spike pairs yield three qualitatively regions with respect to induction of plasticity. Region A (Δt < 0.7 msec): A pulse of glutamate activates the I-cell and E_D. The I-cell releases one pulse of GABA that inhibits E_D. In the meantime, the O-cell receives a pulse of ACh. Because the O-cell has a slower dynamic than the I-cell, by the time the O-cell releases GABA and inhibits the I-cell, the I-cells have already inhibited E_D and no plasticity is induced. Region B (0.7 < Δt < 20.2 msec): ACh activates the O-cell which inhibits the I-cell. The I-cell and E_D receive a pulse of glutamate with a delay Δt. By the time the I-cell and E_D receive the pulse of glutamate, the I-cell is in a hyperpolarized state and cannot release GABA. The feedforward inhibition is cancelled, i.e. no GABA arrives to E_D, and the pulse of glutamate depolarizes E_D, activating NMDARs and allowing enough calcium to enter the cell to induce potentiation. Region C (20.2 < Δt < 38 msec): As the arrival of the Glutamate pulse is delayed, eventually the I-cell will be able to spike and release one pulse of GABA. But because it is still recovering from the inhibition that received from the O-cell, GABA will arrive to E_D later than in Region A. E_D depolarizes just enough for calcium to cross the depression threshold before being inhibited, and depression is induced. **(B)** Single spike-douplets yield four qualitatively regions

with respect to induction of plasticity. Region D ($\Delta t < -6.28$ msec): Similarly to Region A, glutamate is administrated before ACh. Two pulses of glutamate activate the I-cell, which releases 2 pulses of GABA that inhibit E_D. ED cannot depolarize enough to activate enough NMDARs to induce plasticity. Region E ($-6.28 < \Delta t < 0.3$ msec): the I-cell receives 2 pulses of glutamate but only releases 1 pulse of GABA because of the inhibition is receiving from the O-cell. E_D depolarizes enough to allow calcium to cross the depression threshold, and depression is induced. Region F ($0.3 < \Delta t < 18.27$ msec): I-cell receives 2 pulses of glutamate but it does not release any GABA because of the action of the O-cell. E_D depolarizes enough to allow calcium to cross the potentiation threshold and potentiation is induced. Region G ($18.27 < \Delta t < 70$ msec): the I-cell releases either 1 or 2 pulses of GABA, depending on the delay between the 2 pulses of glutamate and the GABA released from the O-cell, which induces depression. The amplitude of depression depends on the either E_D received 1 or 2 pulses of GABA and the time at which these pulses arrive to E_D.

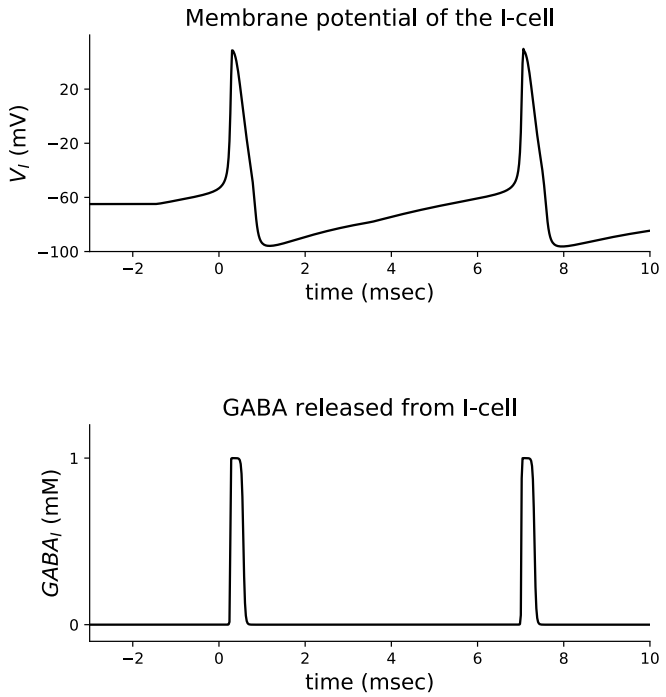

Figure S2: Membrane potential of the I-cell when it receives two pulses of glutamate (with amplitude 1mM and duration of 3 msec) with a frequency of 0.2 msec^{-1}, and respective GABA release. GABA concentration can be described by a square function.

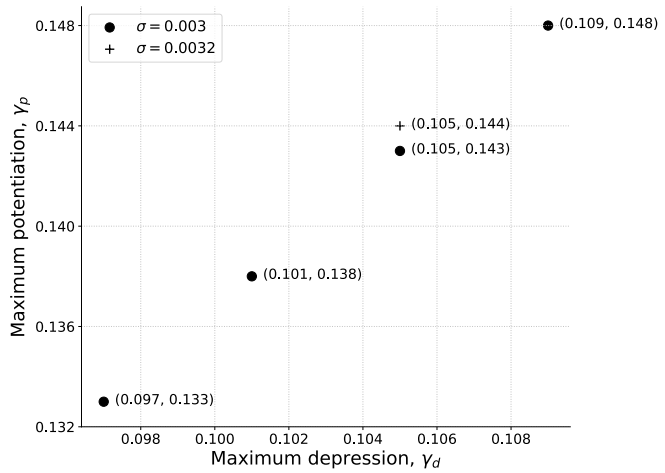

Figure S3: Set of parameters for which we obtain the same results as the ones shown in Fig.4

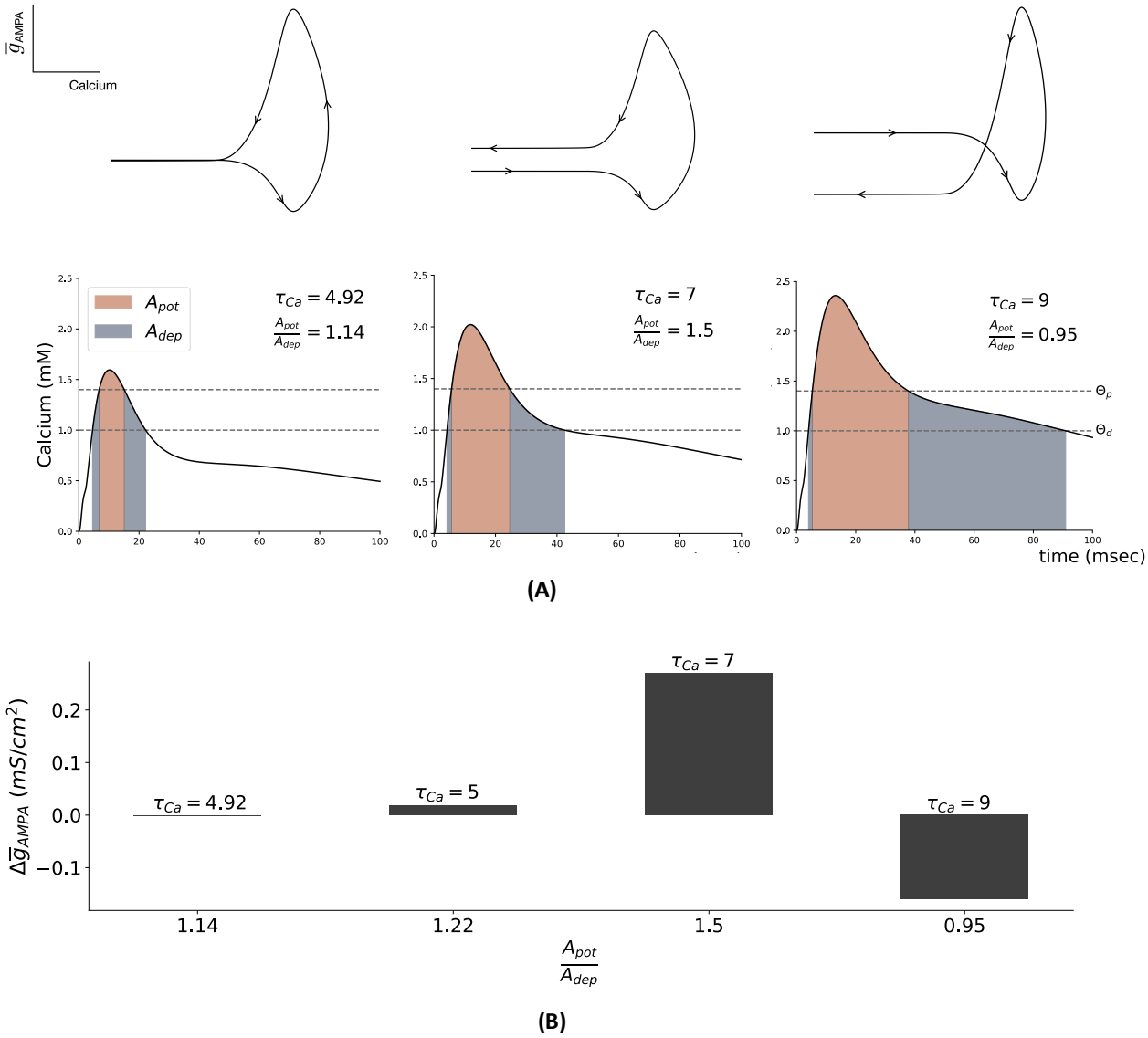

Figure S4 : Increasing the ration between the area of potentiation and depression increases induction of synaptic plasticity. (A) By changing the calcium decay rate τ_{Ca} **,** we change the ratio between the potentiation area (integral of calcium concentration above the potentiation threshold θ_p) and the depression area (integral of calcium concentration above the depression threshold θ_d and bellow the potentiation threshold). **(B)** As the ratio between the potentiation and depression area increases, so does the induction of synaptic plasticity. In these numerical simulations, ED receives a pulse of glutamate followed by a pulse of GABA 2 msec after, each with an amplitude of 1mM and duration of 1 msec. The initial value of $\bar{g}_{AMPA}$ is 1.8 mS/cm^2. All the other parameters are as indicated in Methods. The ratio between the potentiation and depression area is calculated by numerically integrating the area in the potentiation and depression zone, using the trapezoidal method.